Supporting Information

Experimental Section

1. Sample preparation

Synthesis: 0.364 g of V_2O_5 and 0.06 g of polyethylene glycol-400 (PEG) were dissolved in 25 mL of deionized water along with drops of 5 mL of H_2O_2. Following a stirring period of 12 h at 25℃, the mixture was shifted to a 50 mL Teflon-lined autoclave and stored at 180 °C for 60 h. Cleaning of the above-mentioned production several times thoroughly deionized water and anhydrous ethanol, dried in a vacuum oven at 80 °C for 12 h to obtain $V_3O_7{\cdot}H_2O$ nanorods. 0.01 mol of vanadium oxide powders obtained from the above experiments and 0.00125 mol of magnesium carbonate were dissolved in deionized water and stirred for 2 h. The prepared solution by hydrothermal reaction 3 h at 180 °C. $Mg_xV_3O_7{\cdot}H_2O$ material was obtained.

2. Electrochemical measurements

The electrochemical properties of the electrodes were tested using a multichannel electrochemical analyzer (VMP3, Bio-Logic-Science Instruments) NEWARE battery test system and CHI (760E, Chenhua) to carry out the electrochemical performance of the electrode, EIS is performed at an open circuit potential, and the perturbation from 10 kHz to 100 kHz is 5 mV.

3.Assembly of MgVO//Zn and VO//Zn of button cells

For the MgVO//Zn button cells (2032 type), the cathode coating was made of MgVO, PVDF, and super P in the ratio of 8:1:1 and NMP was used as solvent, the prepared coating was then uniformly applied to the carbonaceous material as a collector. The button cells were constructed using a MgVO cathode and solid zinc serves as an anode, in addition, the electrolyte is 3 M Zn $(CF_3SO_3)_2$. The fabrication process for VO//Zn button cells was like the above, with the exception that the cathode was VO instead of MgVO.

4.Characterization

The crystal structures of the material were examined by X-ray diffraction (XRD) (Bruker D8-Advance) with Cu Kα radiation (λ = 0.15406 nm). The microstructure of the cathode

samples was observed using a scanning electron microscope (SEM) equipped with an energy-dispersive X-ray spectroscopy (EDS) detector (SU8010; HITACHI). Transmission electron microscopy (TEM) and high-resolution transmission electron microscopy (HRTEM) were performed on a JEOL 2100 F transmission electron microscope to further analyze the morphology. X-ray photoelectron spectroscopy (XPS) (ESCALAB 250Xi; Thermo Scientific Escalab) with Al-Kα radiation was used as the excitation source to clarify the surface elements and chemical states of MgVO.

Table S1: Comparison table of the energy density of different aqueous Zn ion energy storage devices.

Cathode Materials	E (W·h/kg)	P (W/kg)	Reference
δ-V_2O_5	257 W·h/kg	36 W/kg	1
D-MoS_2	161.3 W·h/kg	55.8 W/kg	2
$CaV_6O_{16}·3H_2O$	210 W·h/kg	70 W/kg	3
$Na_2V_6O_{16}·3H_2O$	90 W·h/kg	15.8 W/kg	4
$V_2O_5·H_2O$	144 W·h/kg	100 W/kg	5
PANI-S	61 W·h/kg	56 W/kg	6
$Sn_{1.5}V_2O_7(OH)_2·3.3H_2O$	191.4 W·h/kg	58.3 W/kg	7

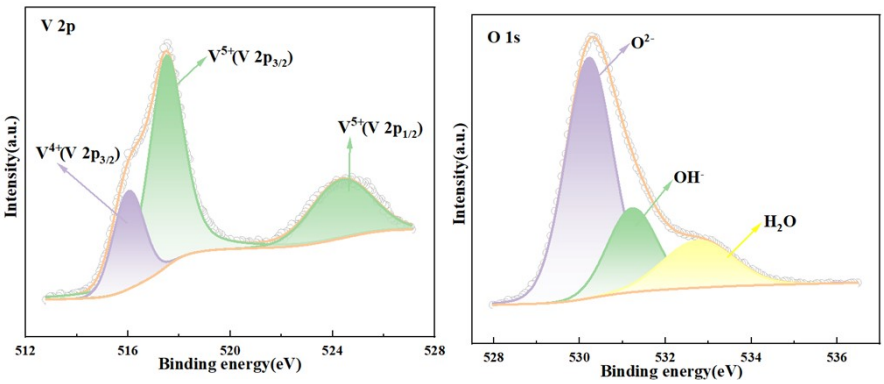

Figure S1: XPS spectra of O 1s and V 2p with VO.

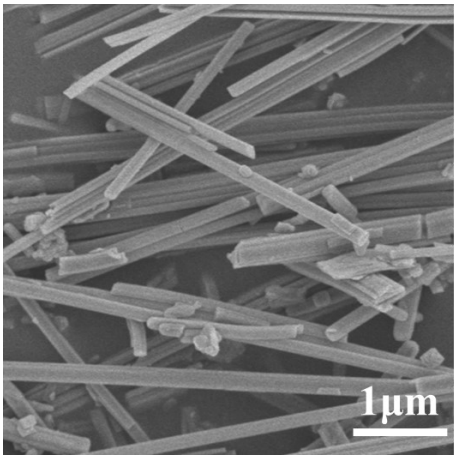

Figure S2: SEM images of VO.

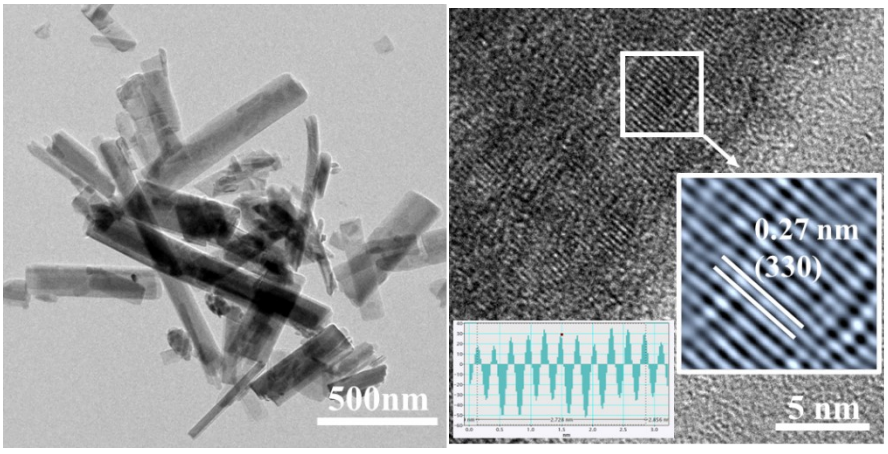

Figure S3: TEM images of VO and HRTEM images of VO.

Note: VO samples (Figure S2) show typical nanorods with diameters reaching about 170 nm (Figure S3), and lengths extending to a few micrometers.

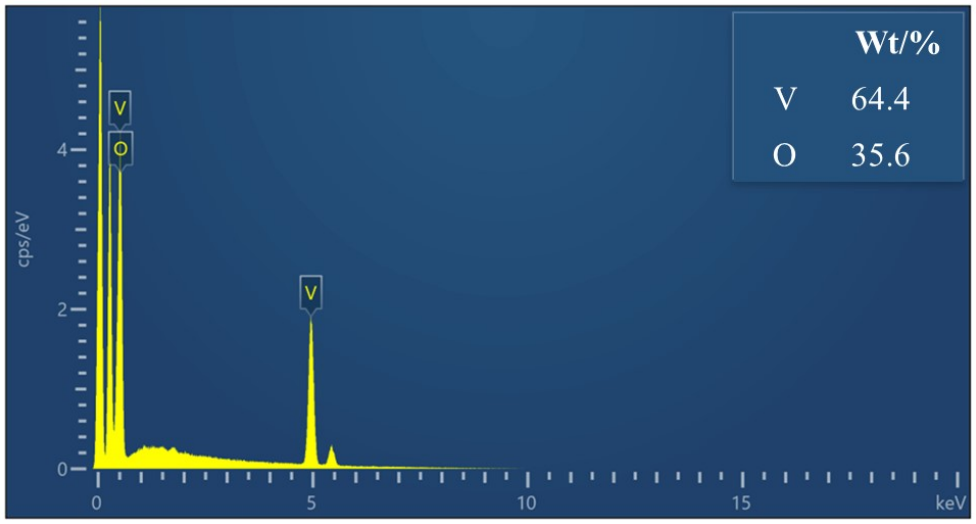

Figure S4: EDS spectrum of VO.

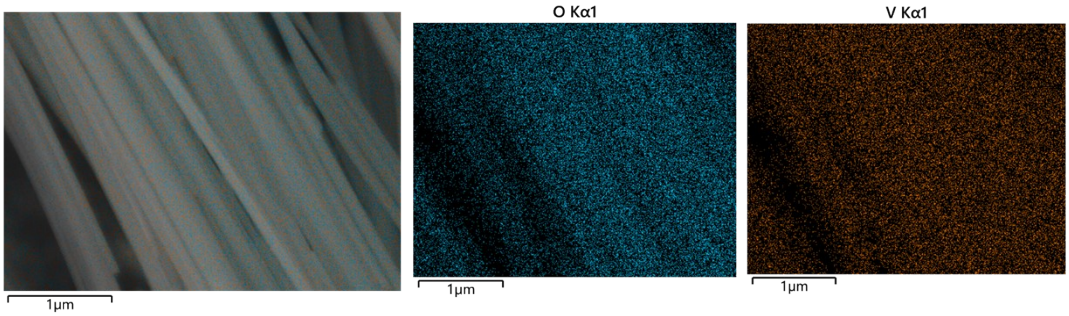

Figure S5: SEM-EDS elemental mapping of VO.

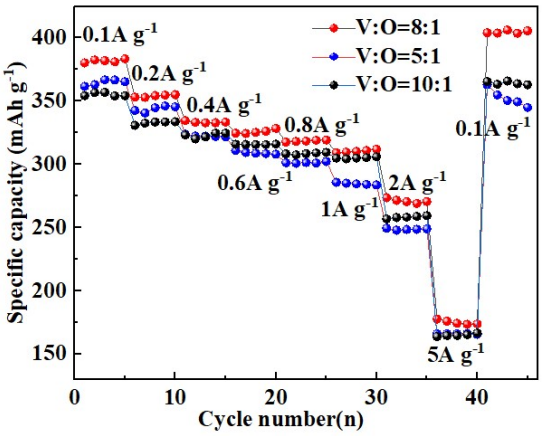

Figure S6: Rate properties of MgVO doped with different molar ratios of Mg^{2+}.

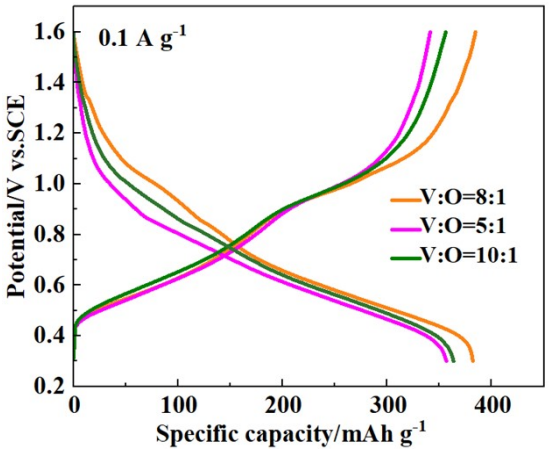

Figure S7: The GCD curves of MgVO at 0.1 A g^{-1} doped with different molar ratios of Mg^{2+}.

Note: We initially explored the effects of different Mg doping ratios on the electrochemical properties of MgVO materials, as illustrated in Figures S6 and S7. Specifically, three MgVO samples with V to Mg molar ratios of 5:1, 8:1, and 10:1 were synthesized using a consistent method. Systematic electrochemical performance testing revealed that the MgVO sample with a V to Mg molar ratio of 8:1 exhibited the most exceptional electrochemical performance in the MgVO//Zn battery. Therefore, the MgVO sample with a V to Mg molar ratio of 8:1 was selected as the optimal representative for an in-depth investigation of its electrochemical properties, relevant characterization techniques, and the underlying mechanisms during electrochemical reactions.

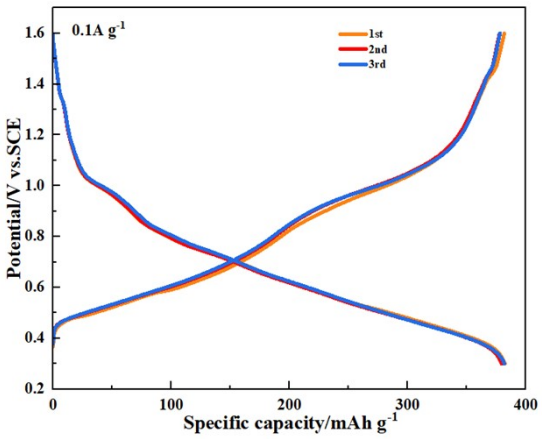

Figure S8: The GCD curves of MgVO at a scan rate of 0.1 A g^{-1}.

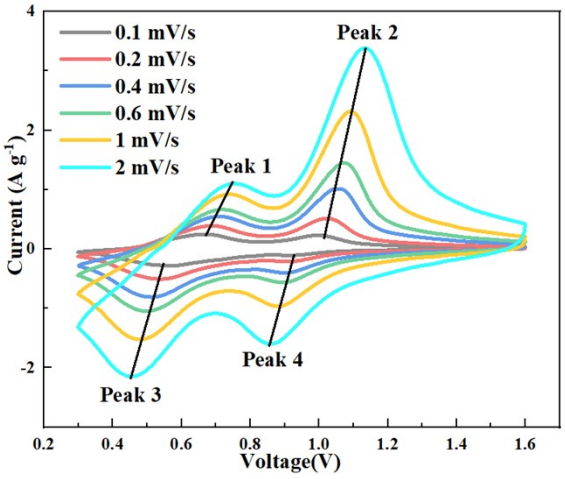

Figure S9: The CV curves at different scan rates.

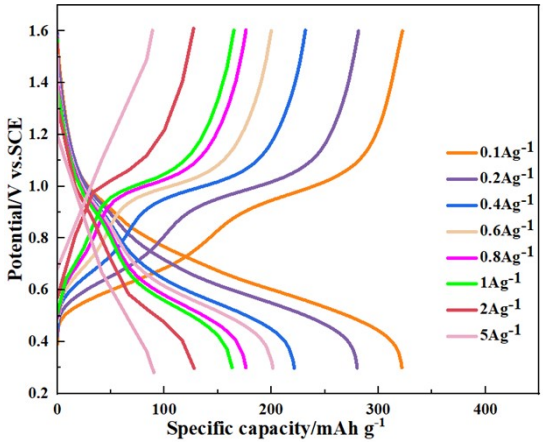

Figure S10: GCD curves of VO at different current densities from 0.1 to 5 A g^{-1}.

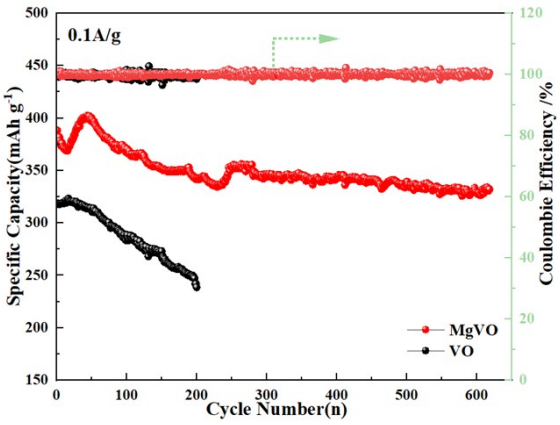

Figure S11: Long-term cycling performance and Coulombic efficiency of VO//Zn and MgVO//Zn battery at 0.1 A g^{-1}.

Note: In contrast, VO's specific capacity decreased to 238.8 mAh g^{-1} after 200 cycles, retaining

only 75% of its initial capacity (Figure S11).

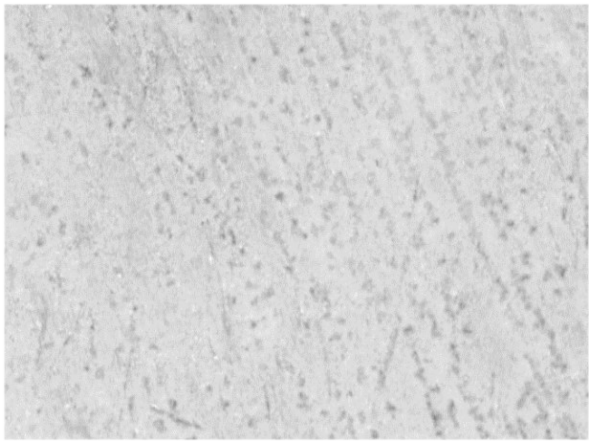

Figure S12: Optical image of the zinc surface after long-term cycling.

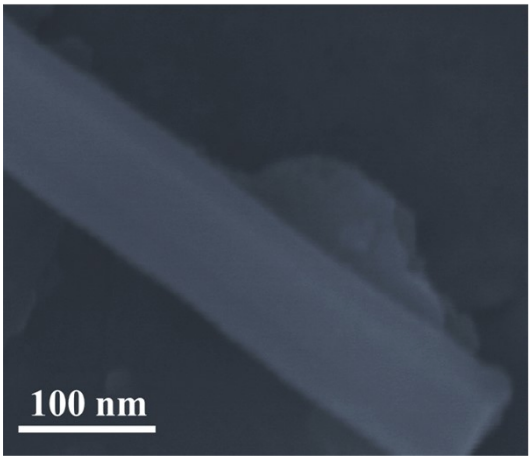

Figure S13: SEM image of MgVO after long-term cycling.

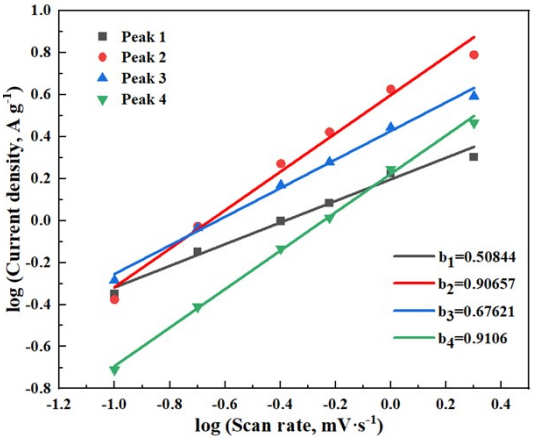

Figure S14: The corresponding plots of log (peak current) vs. log (scan rate) at each peak.

The correlation between peak current *(i*) and scan rate (*v*), and the assessment of the capacitive effect, were analyzed based on the equations provided[8]:

$$i = av^b \quad (1)$$

$$i = k_1 v + k_2 v^{\frac{1}{2}} \quad (2)$$

$$\log(i) = b\log(v) + \log(a) \quad (3)$$

Among these parameters, k_1, k_2, a, and b are variable factors, where k_1 and k_2 denote coefficients associated with capacitive and diffusion control, respectively. Typically, the parameter b ranges between 0.5 and 1, where values closer to 0.5 indicate a stronger influence of diffusion processes, while values closer to 1 suggest predominant capacitive control[9]. For VO, the b values for peaks 1 to 4 (Figure S9) range from 0.51 to 0.91 (Figure S14).

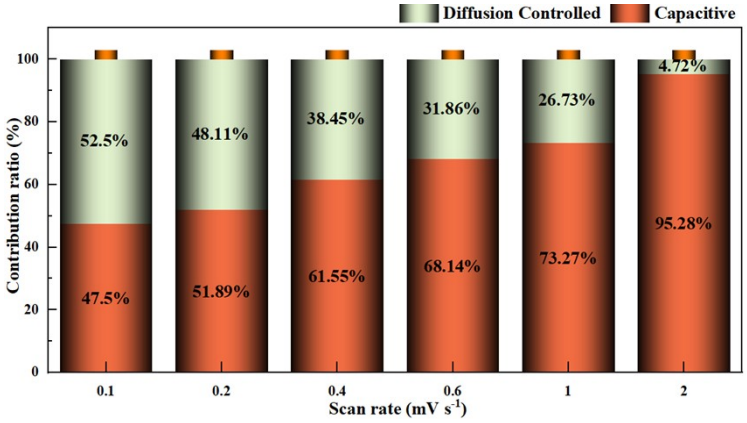

Figure S15: The capacitive contributions of VO at different scan rates in 3M Zn $(CF_3SO_3)_2$ electrolytes.

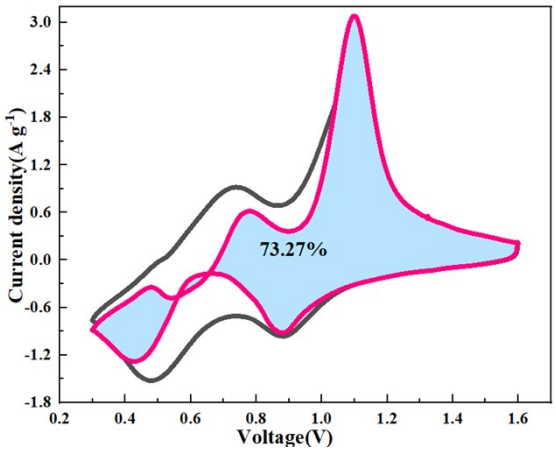

Figure S16: Capacitive contributions to the total current for VO at 1mV s^{-1}.

Reference

1 X. Liu, H. Euchner, M. Zarrabeitia, X. Gao, G. A. Elia, A. Groß, S. Passerini, *ACS Energy Lett.*, 2020, **5, 9**, 2979–2986

2 S. Li, Y. Liu, X. Zhao, K. Cui, Q. Shen, P. Li, X. Qu, L. Jiao, *Angew. Chem. Int. Ed*., 2021, **60**, 20286–20293

3 Y. Zhang, F. Wan, S. Huang, S. Wang, Z. Niu, J. Chen, *Nat. Commun.*, 2020, **11**, 2199.

4 H. Ping, T. Zhu, X. Wang, X. Wei and L. Mai, *Nano Lett.*, 2018, **18**, 1758–1763

5 M. Yan, P. He, Y. Chen, S. Wang, Q. Wei, K. Zhao, X. Xu, Q. An, Y. Shuang and Y. Shao, *Adv. Mater.*, 2017, **30**, 1703725.

6 H. Y. Shi, Y. J. Ye, K. Liu, Y. Song and X. Sun, *Angew. Chem. Int. Ed.*, 2018, **57**, 16359-16363.

7 W. Xu, C. Sun, N. Wang, X. Liao, K. Zhao, G. Yao, Q. Sun, H. Cheng, Y. Wang, X. Lu, *Nano Energy*, 2021, **81**, 105584.

8 J. Wang, J. Polleux, J. Lim, B.Dunn, *J. Phys. Chem. C* 2007, **111**, 14925-14931.

9 Z. Hu, L. Wang, K. Zhang, J. Wang, F. Cheng, Z. Tao, J. Chen, *Angew Chem Int Ed.*, 2014, **53** (47), 12794-12798.